Article

Green Enzymatic Synthesis of Geranyl Butyrate: Process Optimization and Mechanistic Insights

Francisco Simão Neto, Paulo Gonçalves de Sousa Junior, Carlos José Alves da Silva Filho, Lucas Pinheiro Coutinho, Rafael Leandro Fernandes Melo, Javier Rocha-Martin, Maria Alexsandra de Sousa Rios, Ada Amélia Sanders Lopes, Norberto de K. V. Monteiro, Marcos Carlos de Mattos, Leonardo Farias Serafim, and José Cleiton Sousa dos Santos*

Read Online

ACCESS | Metrics & More | Article Recommendations | Supporting Information

ABSTRACT: Flavor esters are organic compounds widely used in the food industry to enhance the aroma and taste of products. However, most chemical processes for the production of these flavoring compounds use toxic organic solvents. Some organic solvents derived from petroleum can leave behind residual traces in food products, which may raise concerns about potential health risks and contamination. In this study, we employ Eversa Transform 2.0, a commercial lipase derived from the lipase from *Thermomyces lanuginosus*, to produce geranyl butyrate in aqueous media. The chemical process was optimized using the Taguchi method, and a conversion of 93% was obtained at the optimal reaction conditions of: 1:5 molar ratio (v/v), 15% biocatalyst load (w/w), at 50 °C, in 6 h. Classic (molecular dynamics) and quantum (density functional theory) simulations unveiled amino acid residues involved in the stabilization of the enzyme−substrate complex. Detailed QM/MM mechanistic studies identified the nucleophilic attack of the deacylation reaction as the rate-limiting step of the entire mechanism, which has a free energy barrier of 14.0 kcal/mol.

1. INTRODUCTION

Flavor esters are organic compounds widely used in the industry to enhance the aroma of products such as soaps, deodorants, and perfumes.[1] These compounds play an essential role in the food industry, where they are used as flavoring agents due to their ability to replicate the natural flavors found in fruits, flowers, and other natural sources.[2] In addition to their versatility, flavor esters contribute to the overall sensory appeal of food and beverages.[3] By using these compounds, manufacturers can tune their product's taste and aroma profiles, making them more appealing to consumers since the unique scent of ester compounds can trigger pleasurable associations and evoke memories, creating a sense of familiarity with the product. However, it is worth noticing that the excessive usage of flavor esters can result in an artificial or overpowering final taste of the product. Regulatory bodies governing food safety and quality control have established guidelines to ensure the responsible and safe use of flavor esters in food production.[4]

Flavor esters can be synthesized through the esterification reaction between an alcohol (acyl acceptor) and an organic acid (acyl donor). The characteristic flavor and scent of the esters produced by this chemical route are directly associated with the chemical nature of the reactants used in the synthesis.[5] For instance, geranyl butyrate exhibits a fruity and

floral scent reminiscent of fresh and tropical fruits such as pineapple, peach, and strawberry.[6] It is formed through the esterification of geraniol, a naturally occurring compound found in various fruits and plants, with butyric acid, as shown in eq 1.

$$ \text{(1)} $$
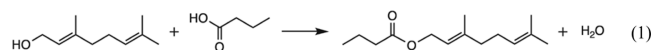
The rate of esterification reactions can vary depending on several factors including: the chemical nature of the reactants, their respective concentrations, the temperature and pressure of the reaction medium, and other factors. Generally, esterification reactions are relatively slow compared with other chemical reactions. To overcome this challenge, using enzymatic catalysis is essential for the feasibility of some industrial processes.[7] These biomolecules work as natural catalysts, increasing the speed of chemical reactions while reducing the formation of unwanted byproducts. Additionally,

these catalysts are considered environmentally friendly, and their biochemical reactions deliver natural products in terms of their origin, which is very attractive to the food industry.[8] Moreover, when enzymes are disposed of in the environment, they are readily broken down into amino acids by natural processes such as microbial activity, oxidation, and hydrolysis.[9]

Among all types of enzymes, those belonging to the lipase family, also classified as hydrolases, are very commonly applied to biotechnological processes.[10] Lipases are enzymes that catalyze the hydrolysis, esterification, and transesterification of lipids and are commonly found in many living organisms. The remarkable affinity of lipases for different types of substrates and their ability to function in acidic or alkaline conditions make these biocatalysts ideal for synthesizing biofuels, detergents, food, and other products.[11] Regarding their structure, most lipases have an additional hydrophobic lid domain, an α/β hydrolase fold, and a Ser-His-Asp/Glu catalytic triad, as shown in Scheme 1.[12]

Scheme 1. (a) Opening of the Lid Domain of the Lipase (*Tl*L) Exposing the Active Site to Substrates. (b) General Acylation and Deacylation Mechanisms of Lipases
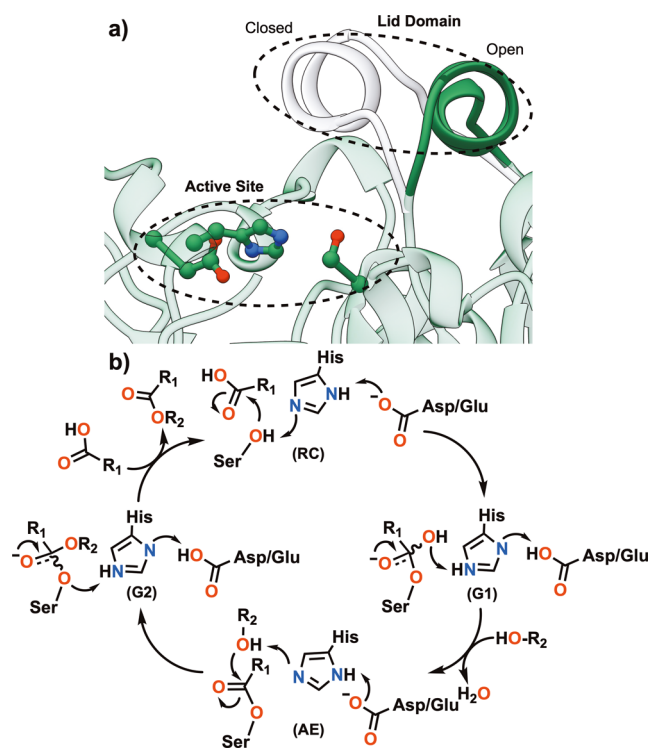
Under minimal substrate concentration, the lid domain, which envelops the active site in the resting state, moves apart via conformational changes at the oil/water interface, making the active site accessible to substrates.[13] Once at the active site, the substrate can undergo catalysis through a mechanism comprised of two consecutive processes: acylation and deacylation.[14] In the acylation process, the serine amino acid residue from the active site promotes a nucleophilic attack on the electrophilic carbon atom of the substrate. This process fixes the substrate through a covalent bond, generating an acyl−enzyme complex intermediate. In the second step (deacylation), a free nucleophile (HO-R) promotes a nucleophilic attack onto the acyl−enzyme complex intermediate, releasing the products and regenerating the enzyme.

Eversa Transform 2.0 (ET2) is the commercial name of the lipase from *Thermomyces lanuginosus* (*Tl*L) (previously *Humicola lanuginosa*), produced by Novozymes through the submerged fermentation of a genetically modified strain of *Aspergillus oryzae*, with high specificity for raw materials and high activity at mild process conditions.[15] The ET2 enzyme is an extremophilic lipase capable of functioning under extreme temperature and pressure conditions. It has a low production cost (15 US\$/kg) and contains 269 amino acid residues, a molecular mass of ∼30 kDa, and an activity of 9100 IU/mL.[16] This enzyme has been used as a catalyst in many chemical reactions, such as the enzymatic esterification of glycerol,[17] the synthesis of biolubricants,[18] the production of biodiesel from the esterification of babassu oil (*Orbignya* sp.),[19] and the production of esters using tucuman oil (*Astrocaryum vulgaris*).[20]

Along with the utilization of biocatalysts, experimental planning is an essential aspect of optimizing chemical processes, as it allows the determination of the most efficient experimental conditions. The Taguchi methodology is an experimental planning and process organization technique that aims to improve product quality and production efficiency.[21] It was developed by the Japanese engineer Taguchi in the 1950s and has gained widespread popularity in various industries due to its effectiveness in achieving robustness and cost reduction while minimizing the number of experiments. The first step of this methodology involves the identification of key performance metrics or response variables that must be optimized. Next, the factors, which are the variables or parameters that can potentially influence the response variables, are selected. Each factor is then assigned a set of levels or values, chosen based on the range of practical values and the desired sensitivity used during the experimentation. Depending on the number of factors and levels considered, an orthogonal array is chosen to ensure an efficient and balanced allocation of factor combinations. Using the chosen orthogonal array, experiments are conducted to collect data on the response variables. Each experiment consists of a specific combination of factor levels, and multiple replications are typically performed to account for variability. Finally, signal-to-noise ratio (S/N) and variance (ANOVA) analyses are performed to interpret the experimental data and identify the significant factors affecting the response variables. Once the optimal factor level is identified, a confirmation experiment is conducted to validate the results and ensure the robustness of the obtained solution.

Since some molecular factors controlling chemical reactions cannot be determined experimentally, computational chemistry provides useful tools to study chemical reactions and predict important thermodynamic and kinetic parameters.[22] One powerful approach in computational chemistry for studying enzymatic reactions is the quantum mechanics/molecular mechanics (QM/MM) method.[23] This technique combines the accuracy of quantum mechanical calculations with the efficiency of molecular mechanics force fields to capture the electronic and structural features of the active site of the enzyme and its surrounding environment. In QM/MM calculations, the active site where the reaction occurs is treated quantum mechanically to accurately describe the electronic behavior of the reacting species. In contrast, the rest of the enzyme and solvent molecules are treated using molecular mechanics to account for their bulk effects. This hybrid approach accurately represents the enzyme's active site and the surrounding environment, providing insights into the reaction

mechanism, transition states, reaction energetics, and various aspects of enzyme catalysis.[24]

This work presents an optimized synthetic route to produce the flavor ester geranyl butyrate from the enzymatic esterification of geraniol and butyric acid catalyzed by the Eversa Transform 2.0 (ET2). In contrast to previous reports, we performed an esterification reaction rather than an acyl–transfer reaction.[5,7] By applying the Taguchi method, the effect of the molar ratio (MR) of the reactants, the temperature, the reaction time, and the biocatalyst load on the conversion was evaluated. The reaction product was characterized by multiple chromatographic techniques and nuclear magnetic resonance (NMR) spectroscopy. Finally, using a combination of classic [molecular docking and molecular dynamics (MD)] and quantum [density functional theory (DFT)] computational methods, structural, kinetic, and thermodynamic data of the esterification reaction were obtained and are in excellent accordance with the experimental observations.

2. MATERIALS AND METHODS

2.1. Biocatalyst and Chemical Reagents. The commercial lipase Eversa transform 2.0 (ET2) from *T. lanuginosus* (*Tl*L), produced by Novozymes through the submerged fermentation of a genetically modified strain of *A. oryzae*, was purchased from Sigma-Aldrich Brazil Ltd. (Cotia, São Paulo, Brazil). The chemical reagents used were analytical grade from Synth (São Paulo, Brazil) and Vetec (São Paulo, Brazil). The Statistica 10 software (Statsoft, USA) was used for the experimental design based on the Taguchi method.

2.2. Enzymatic Activity Assay. Following the experimental design assessments, the activity assay was carried out with reaction mixtures containing different ratios of reagents, at different temperatures, and for different time intervals. Vials of 2 mL were used to perform biochemical reactions under a controlled incubator temperature, in addition to maintaining an orbital agitation of 200 rpm. After completion of the esterification reaction, the samples were analyzed in duplicate in two Erlenmeyer flasks with 0.2 g of the sample, 5 mL of standard ethyl alcohol, and 3 drops of phenolphthalein as the indicator. Each sample was titrated with a 0.1 M NaOH solution until the color changed to a subtle pink. After titration, the total consumed volume was used in eq 2 to obtain the acidity index (AI).

$$AI = \frac{MW_{NaOH} \cdot M_{NaOH} \cdot f \cdot V_{NaOH}}{m} \quad (2)$$

In eq 1, MW_{NaOH} is the molecular mass of NaOH, M_{NaOH} is the molarity of the NaOH solution used in the titration, f is the correction factor determined by NaOH standardization, V_{NaOH} is the total volume of NaOH consumed during the titration, and m is the mass of the analyzed sample. The conversion (X) of butyric acid into the flavor ester geranyl butyrate is then given by eq 3, where AI_0 represents the initial acidity value due to the starting concentration of acid in the sample, and AI represents the final acidity value, equivalent to the remaining acid in the solution, not consumed during the enzymatic reaction.

$$X \ (\%) = \frac{AI_0 - AI}{AI_0} \times 100 \quad (3)$$

2.3. Quantification and Characterization of the Products. The sample obtained from the optimal conversion

point was analyzed by high-performance liquid chromatography using a Shimadzu LC-18 column at a temperature of 25 °C equipped with a UV detector. A retention time of 5.5 min was observed for the product in the injected sample (1 mg/mL), as shown in Figure S1. The eluent was a mixture of acetonitrile and water in a 4:1 (v/v) ratio, with a flow rate of 3.0 mL/min for 5 min. The wavelength of 220 nm was chosen for the analysis, which showed the highest absorption. The one-dimensional hydrogen (^1H NMR) and carbon (^{13}C NMR) NMR spectra were recorded in a Bruker spectrometer, model Advance DRX-300, belonging to the northeast center for application and use of NMR, located at the Federal University of Ceara (CENAUREMN-UFC). The experiment was carried out at a hydrogen atom frequency of 300 MHz and a carbon atom frequency of 75 MHz. All samples were dissolved in deuterated chloroform ($CDCl_3$) and analyzed in 5 mm NMR tubes.

2.4. Experimental Design and Statistical Analysis. An experimental design based on the Taguchi method was used with a standard L9 orthogonal matrix (the "L" and "9" represent the Latin square and the number of experiments, respectively) to distribute four factors in three levels to maximize the conversion. The four independent factors: the molar ratio between organic acid and alcohol (MR), the biocatalyst load (Cat), the temperature (T), and the reaction time (t), as well as their corresponding levels, are shown in Table 1. The biocatalyst load was calculated from the reaction

Table 1. Experimental Procedure Levels and the Range of Independent Factors[a]

levels	MR	Cat (% w/w)	T (°C)	t (h)
level 1 (L1)	1:1	5	30	2
level 2 (L2)	1:5	10	40	4
level 3 (L3)	1:9	15	50	6

[a]The chosen parameters were the molar ratio of acid: alcohol (MR), the biocatalyst load (Cat), the temperature (T), and the reaction time (t).

volume after the calculation of the MR. The values of S/N ratios (signal-to-noise) corresponding to the conversions were calculated using the characteristics of the "bigger is better" function since the objective of this study is to maximize the response (flavor ester production). In the Taguchi method, the S/N ratio measures quality characteristics and the deviation from the desired value. Thus, using the S/N ratio to analyze the results reduces the system's sensitivity to sources of variation, resulting in good performance. The value of the S/N ratio for each experiment was calculated according to eq 4.

$$S/N = -10 \log \left(\frac{1}{n} \sum_{i=1}^{n} \frac{1}{y_i^2} \right) \quad (4)$$

In eq 4, y is the fatty acid conversion for the corresponding sample, i is the number of replicates, and n is the number of responses for the combination of factor levels in any given parametric combination. The predicted signal-to-noise $(\widetilde{S/N})$ ratio under optimal conditions for obtaining the maximum conversion was estimated by eq 5.

$$\widetilde{S/N} = \frac{\overline{S}}{N} + \sum_{i=1}^{n} \left(\frac{S}{N_j} - \frac{\overline{S}}{N} \right) \quad (5)$$

In eq 5, $\overline{S}/N$ is the arithmetic mean of all S/N ratios, S/N_j is the S/N ratio at the sweet spot for each factor, and n is the number of factors that significantly affect the process.

2.5. Computational Modeling and MD Simulations.
The computational model of ET2 was based on the original structure of the lipase from *T. lanuginosus* (*Tl*L, PDB identification code: 1EIN).[25] The geometry of the substrates butyric acid and geraniol was optimized at the B3LYP/6-311G +(d,p)/D3 level of the DFT without any geometric constraints using the Gaussian software package.[26] Their charges and electrostatic potentials (ESP) were computed at the same level of theory, and their force field parameters were developed using the antechamber software from the AmberTools package.[27] The enzyme−substrate complexes were built through molecular docking using AutoDock Vina 1.5.6 software.[28] In the rigid docking protocol utilized, the structure of the enzyme was kept fixed, but the substrates were allowed to adopt any conformations. This procedure provided 20 poses, which were ranked based on their energies. The three poses with the lowest energies for each substrate were selected for all-atom MD simulations.

The MD simulations were performed using the GRO-MACS[29,30] program utilizing the AMBER ff19SB force field.[27] The enzyme−substrate complex was placed in a cubic box with dimensions of $10 \times 10 \times 10$ nm. The shortest distance from the edge of the box to the surface of the complex was less than 1 nm. The particle mesh Ewald method was used to compute the electrostatic interactions, and for both Coulombic and van der Waals interactions, a 1.2 nm cutoff distance was established. The TIP3P[31] water model was used as the solvent, and Na^+ and Cl^- ions were added to neutralize the total charge of the system. The system was then energy-minimized for 3000 steps using the steepest descent algorithm before each MD simulation. The MD simulations were performed using a constant number of particles (N), pressure (P), and temperature (T) as an NPT ensemble for a total of 100 ns. The trajectories were computed for each model with a time step of 1 fs. Finally, cluster analysis was performed to obtain the most representative structure.

2.6. Hybrid Quantum Mechanics and Molecular Mechanics Calculations.
The hybrid two-layer QM/MM (ONIOM) calculations were performed by using the Gaussian software package. This method utilizes a subtractive method in which the MM energy $[E_{MM}(model)]$ of the QM(model) part is subtracted from the sum of the QM energy of the model $[E_{QM}(model)]$ and MM energy $[E_{MM}(total)]$ of the whole (total) system, as shown in eq 6.

$$E_{QM/MM}(total) = E_{MM}(total) - E_{MM}(model)$$
$$+ E_{QM}(model) \tag{6}$$

This subtraction method corrects the artifacts introduced by using link atoms. The ONIOM optimization procedure uses macro/microinteractions, and the electrostatic interactions between the QM and the MM part were treated by mechanical embedding. The QM region (model) was defined as the catalytic triad (Ser_{146}, His_{258}, and Asp_{201}), the second coordination shell residue Tyr_{21}, and the substrates. It contains a total of 51 atoms in the acylation mechanism and 77 atoms in the deacylation mechanism, with a -1 charge on each system. The remaining atoms of the system were treated in the classic MM region. The QM region was optimized without any geometric constraint by using the hybrid B3LYP exchange−

correlation DFT functional. The 6-31G(d,p) basis set was used to implement the computations, and Grimme's function with the Becke−Johnsons damping effect (GD3BJ) was used to take into account the dispersive effects. Hessians were calculated at the same level of theory as those of the optimizations to confirm the nature of the stationary points along the reaction coordinate. The transition states were confirmed to have only one imaginary frequency corresponding to the reaction coordinates. Single-point calculations were performed using the larger 6-311+G(d,p) basis set with the B3LYP and M06-2X functionals (Figure S4). In these calculations, the electrostatic interactions between the QM and the MM parts were treated by electronic embedding. Zero-point vibrational, thermal, and entropy corrections were added to the final energies (at 298.15 K and 1 atm). The MM region was modeled using the AMBER force field as implemented in Gaussian software.

3. RESULTS AND DISCUSSION

3.1. Process Optimization by the Taguchi Method.
The application of the Taguchi method for the optimization of the biochemical process allowed for the determination of all parameters affecting the conversion of the chemical reaction by performing a minimum number of experiments. In addition, a variation in the interaction between each parameter was also evaluated to determine the best level of each parameter that ensures the optimal conversion point within the chosen variable range. Table 2 presents, in an expanded form, the

Table 2. Experimental Design of the Taguchi L9 Plan[a]

experiment	MR	Cat (% w/w)	T (°C)	t (h)	X (%)	S/R
1	1:1	5	30	2	15.2 ± 0.5	23.61
2	1:1	10	40	4	56.5 ± 0.7	35.04
3	1:1	15	50	6	90.1 ± 0.2	39.09
4	1:5	5	40	6	75.8 ± 0.6	37.59
5	1:5	10	50	2	50.9 ± 0.3	33.95
6	1:5	15	30	4	53.8 ± 0.3	34.61
7	1:9	5	50	4	66.1 ± 0.8	36.40
8	1:9	10	30	6	64.6 ± 1.5	36.20
9	1:9	15	40	2	33.8 ± 0.2	30.59

[a]All chemical reactions were performed in triplicate to ensure that the error was within the standard limits. A constant orbital agitation of 190 rpm was maintained during the reaction process.

results of the experimental planning, including the conversion values for each point analyzed. By inspecting Table 2, it is easy to notice that the reaction time was the parameter that most influenced the process, positively affecting the formation of the flavor ester. As can be inferred from experiments 3 and 4, a long reaction time is associated with a high conversion rate since both experiments performed for 6 h displayed the highest conversions among all 9 experiments. On the contrary, experiments 5 and 9, with a total reaction time of 2 h, displayed a very low reaction yield despite the use of a high catalyst load (10 and 15% w/w). A similar trend can be observed for the temperature. For instance, experiments 3 and 7, which exhibited the highest and the third highest conversion (90.1 and 66.1%, respectively), were performed at the highest temperature level of 50 °C. These results emphasize the significance of the temperature in increasing the system's kinetic energy, enabling a more significant fraction of the molecules to surpass the activation energy barrier. It also

indicates that the catalyst employed can withstand high temperatures without losing catalytic activity.

On the other hand, the MR and the catalyst load were the factors that least influenced the conversion. In most enzymatic processes, the employed concentration of acyl donors is higher than the concentration of acyl acceptors. However, a high concentration of acid (acyl donor) in esterification reactions may lead to reduced activity or even inactivation of the enzyme due to the changes in pH, which is a known disadvantage of this chemical route. For this reason, the concentration of the acid was kept constant while the concentration of the alcohol was increased. Nevertheless, since the alcohol molecules react with the acyl−enzyme intermediate rather than the enzyme in its native form, a high concentration of alcohol creates competition for the enzyme's active site during the acylation step. Such interactions between the enzyme's active site and the alcohol molecules create complexes that are not catalytic competent, which negatively impacts the reaction rate. A similar pattern of inhibition by alcohols was observed in similar biochemical reactions performed by *Pseudomonas cepacian*,[32,33] *Candida rugosa*,[34] and *Candida antarctica*.[35]

A similar behavior was observed for the catalyst load. Although a high enzyme concentration contributes to the rapid formation of enzyme−substrate complexes, which increases the reaction rate, excessive enzyme amounts can lead to aggregation, preventing substrate binding to the active site. It is noteworthy to emphasize that the optimal MR and catalyst load levels are below the maximum level. This fact holds economic significance since the quantities of raw materials employed in a chemical process directly influence the ultimate cost of the final product.

3.2. Statistical Analysis. The Taguchi method utilizes signal-to-noise (S/N) ratio values to determine the significance of each parameter analyzed. The present study applied the "bigger is better" function to identify these ratios from the conversion values. The information on the average S/N of all levels of each factor, in addition to the delta values, is shown in Table 3 and Figure 1. The delta value results are obtained by

Table 3. Response to Mean S/N Ratios and Order of Variables for the Molar Ratio (MR), the Biocatalyst Load (Cat), the Temperature (T), and the Reaction Time (t)

factor levels	MR	Cat	T	t
1	32.58	32.53	31.47	29.38
2	35.38	35.07	34.40	35.35
3	34.39	34.76	36.48	37.63
delta	2.80	2.53	5.01	8.25

subtracting the factor with the highest S/N value from the factor with the lowest S/N value. This type of analysis utilizes the delta value to rank the factors and define their significance for the process. As already expected, the analysis of Table 3 shows that the reaction time and temperature stood out among the other analyzed parameters, with delta values of 8.25 and 5.01, respectively.

The analysis of the variance provided an analogous outcome. The values obtained in this analysis are presented in Table 4, where the main highlight is given to the p-value, which is the value that determines the significance of the factors during the studied reaction. The significance of a specific parameter is linked to its p-value, which can guarantee up to 95% confidence, provided that this value is less than 0.05. The
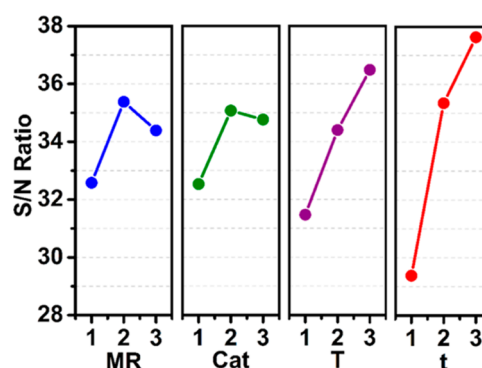

Figure 1. S/N responses for each independent parameter at each level. The MR is shown in blue, the biocatalyst load (Cat) is shown in green, the temperature (T) is shown in purple, and the reaction time (t) is shown in red.

reaction time and the temperature showed significance within the best reliability range, as they presented p-values equal to 0.0004 and 0.0037, respectively, whereas the MR and the catalyst load presented p-values much higher than 0.05. It is important to note that the contribution from the reaction time is about three times more significant than that of the temperature, representing 74.64 versus 23.49% of the total conversion.

Since the statistical analysis indicated that the reaction time (t) was the most influential parameter affecting the conversion, 2D contour surface graphs were generated to study the correlation effect of time with the other variables. The contour plots shown in Figure 2 connect points of equal values of conversion, which can unveil interactions between two distinct factors.

For instance, the temperature and reaction time are positively correlated. That indicates that a concurrent increment of both the temperature and reaction time produces an increment in conversion, although, as can be noted by the inclination of the contour lines toward the reaction time, an increment in the reaction time is more prevalent than an increment in the temperature. The relationship between the MR and the time, on the other hand, exhibits a different behavior. The high conversion contour lines are displayed at reaction time levels above two and MR levels below two. At MR levels higher than two, a decrease in conversion of at least 20% is expected due to the inhibition of the enzyme. Finally, the contour lines for the catalyst load displayed the lowest level of interaction with the reaction time. At reaction times close to level 3 (6 h), a conversion of at least 75% is predicted despite the level of catalyst load.

Based on the data obtained from the Taguchi method, it was possible to derive an equation that expresses the conversion as a function of each of the independent parameters, as shown in eq 7

$$X\ (\%) = 0.11A + 0.691B + 1.209C + 10.97D - 43.5$$
$$(7)$$

In eq 7, X is the conversion for the esterification reaction, and A, B, C, and D are the encoded values of the MR, the biocatalyst load, the temperature, and the reaction time, respectively. The statistical analysis also concluded that the best time was presented in level 3, as 6 h (L3), the best temperature was 50 °C (L3), an adequate biocatalyst load was defined as 15% (L3), and finally, the MR stood out in level 2,

Table 4. Results of Analysis of Variance (ANOVA) for Parameters That Affect the Production of the Flavor Ester

factors	SS	DF	IN	F value	p-value	contribution (%)
molar ratio	60,620	2	30,310	0.05	0.8351	0.03
biocatalyst	73,607	2	36,803	3.01	0.1575	1.84
temperature	879,167	2	439,583	36.95	0.0037	23.49
time	2916,847	2	1,458,423	127.71	0.0004	74.64
total	3,930,241	6				100.00
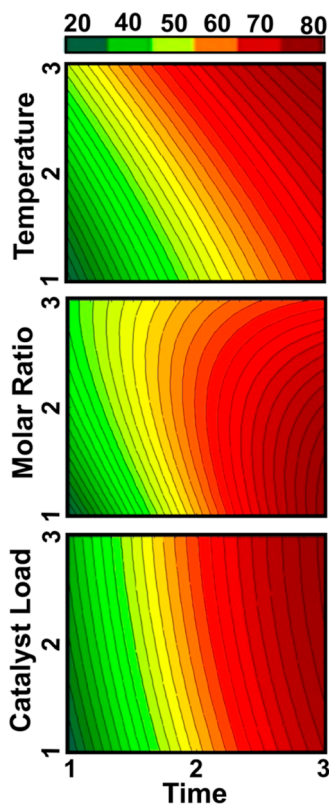
Figure 2. Contour surfaces for the production of geranyl butyrate. The temperature (T), the MR, and the catalyst load (Cat) are evaluated against the reaction time (t), the most influential parameter affecting the conversion.

in a ratio of 1:5 (L2). Equation 7 predicts a conversion of 96% at the optimal parameter conditions. Figure 3 shows the parity plot comparing the predicted response from eq 7 to the response values for the conversion obtained in the experiments.
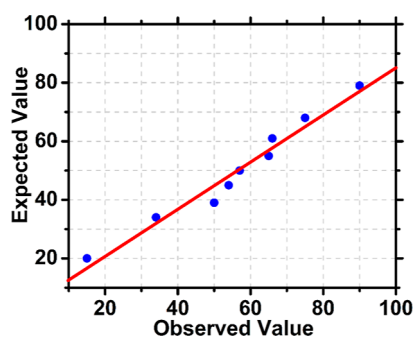

Figure 3. Parity graph evaluating the observed responses versus expected responses provided by eq 7.

3.3. Characterization of Geranyl Butyrate.

The peak observed in the chromatogram shown in Figure S1 is related to the reaction product, geranyl butyrate. The maximum absorption for geranyl butyrate was observed at 220 nm, and the intensity of the peak indicates that the flavor ester was produced in a significant amount, with the concentration of the sample being equivalent to 40 mg/mL.

The ^{1}H NMR spectrum, shown in Figure S2, displays characteristic peaks assigned to the hydrogen atoms of the ester structure. The doublet observed at δ 4.1 ppm (Figure S2a) is related to the methylene hydrogen atoms directly linked to the oxygen atom of the ester functional group. The triplet peak observed at δ 2.3 ppm (Figure S2b) is assigned to the methylene hydrogen atoms bonded to the ester carbonyl carbon atom. The peaks referring to chemical shifts at δ 5.1 and δ 5.4 ppm are attributed to hydrogen atoms linked to sp^2 carbons.

The ^{13}C NMR spectrum, shown in Figure S3, was also used to track the conversion of the alcohol into the flavor ester by the appearance of the carbonyl carbon atom, which resonates at δ 177 ppm. The peaks in the range of δ 130−140 ppm refer to dehydrogenated sp^2 carbons linked to the methyl branch. Vinyl carbons at δ 123 and 124 ppm have very close chemical shifts due to the similarity of the structural profiles of the two carbon atoms (both have chemically similar neighborhoods). The peak with a chemical shift close to δ 60 ppm is attributed to the carbon linked directly to the oxygen of the ester group.

3.4. Computational Modeling and the Mechanism of the Reaction.

The active site of ET2 is composed of a catalytic triad formed by residues Ser$_{146}$, His$_{258}$, and Asp$_{201}$, as shown in Figure 4. Substrates with appropriate conformations and chemical affinity with the residues present in the vicinity of the active site can bind and undergo catalysis. In the enzyme−substrate complex (ET2-BA) obtained by molecular docking and MD simulations, the second coordination shell residue Tyr$_{21}$ stabilizes and orients the BA molecule toward the nucleophilic residue Ser$_{146}$ through hydrogen bonding (H$_T$−O$_C$ = 1.53 Å). The hydrophobic carbon chain of BA interacts with the side chain of residues Ile$_{94}$, Leu$_{154}$, and Phe$_{265}$ through weaker nonpolar interactions. These interactions are responsible for retaining the ET2-BA complex together, as shown by the low rmsd displayed during the course of 100 ns of simulation.

The most representative structure of the catalytic competent ET2-BA complex (R_A), obtained by cluster analysis of MD simulations and optimized by hybrid QM/MM calculations, is shown in Figure 4 inset (a) and in Figure 5. Key bond lengths are shown in Table S1. In R_A, the electrophile−nucleophile (O$_S$−C$_B$) distance is 2.78 Å. The hydrogen atom H$_S$ of the nucleophilic residue Ser$_{146}$ is participating in a hydrogen bond network that connects it with the residues His$_{258}$ and Asp$_{201}$.

The first and rate-limiting step of the acylation reaction involves the nucleophilic attack of the O$_S$H$_S$ side chain of Ser$_{146}$ onto the electrophilic carbon atom C$_B$ of BA. This
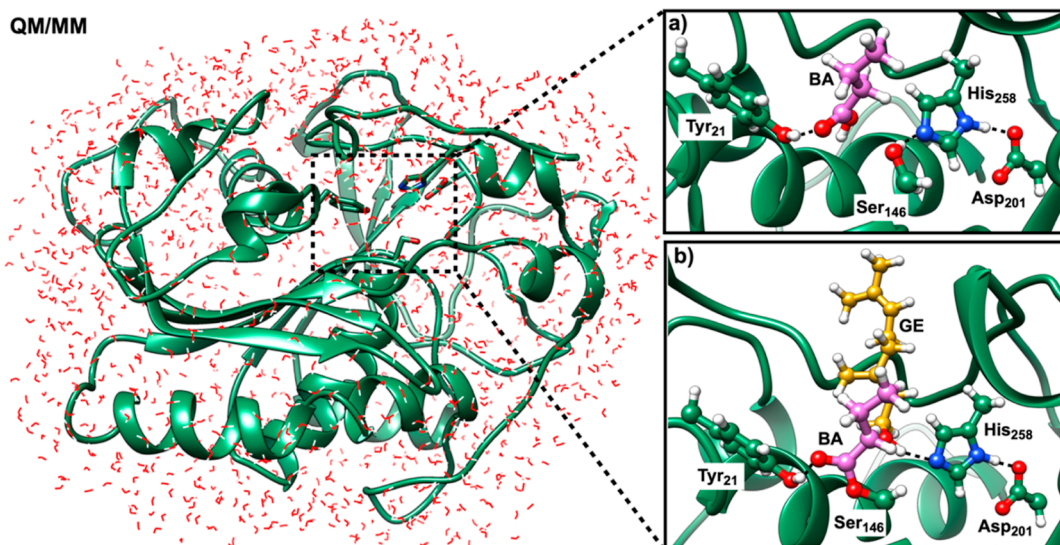
Figure 4. Computational model of ET2 showing explicit TIP3P water molecules (left). The active sites of ET2 in complex with butyric acid (BA) and acyl-ET2 in complex with geraniol (GE) are shown as insets (a,b).
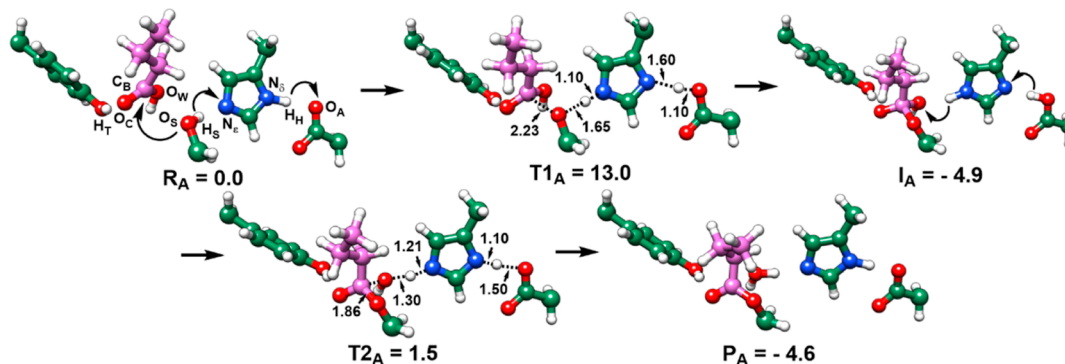

Figure 5. Mechanism of the Acrylation of BA Catalyzed by ET2. The carbon atoms of the substrate (BA) are shown in purple, while the enzyme atoms are shown in green. All bond lengths are displayed in angstroms, and free energies are in kcal/mol (B3LYP), relative to R_A.
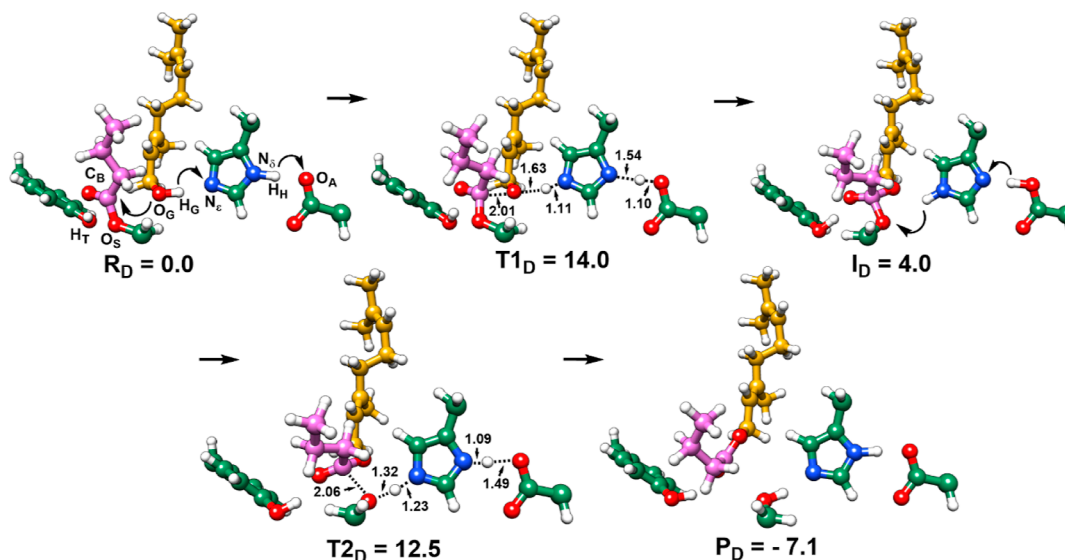

Figure 6. Mechanism of the deacylation of BA and geraniol catalyzed by acyl-ET2. The carbon atoms of BA, geraniol, and the enzyme are shown in purple, yellow, and green, respectively. Bond lengths are displayed in angstroms and free energies in kcal/mol (B3LYP), relative to R_D.

process takes place with a free energy barrier of 13.0 kcal/mol and is associated with $T1_A$. In the structure of transition state

$T1_A$, the electrophile-nucleophile ratio is decreased to 2.23 Å. This step also involves two proton transfer events (O_S−H_S to

H_S-N_ε and $N_\delta-H_H$ to H_H-O_A) which invert the protonation state of His_{258}. The gem-diol intermediate I_A generated after this step is exergonic by 4.9 kcal/mol. This unstable intermediate collapses with a very low energy barrier (6.4 kcal/mol), which is associated with $T2_A$. The collapse of I_A takes place with the same proton transfer events as in $T1_A$ but in the opposite direction. The product of the acylation reaction (P_A) is the acyl enzyme (acyl-ET2), where the butyric group (butyrate) is added to the Ser_{146} side chain and a free water molecule.

The second process involved in the production of the flavor ester geranyl butyrate is deacylation. In this process, the acyl-ET2 enzyme binds the second substrate, a molecule of geraniol (GE), to form the second enzyme−substrate complex, acyl-ET2-GE, shown as R_D in Figure 6.

In the first step of the deacylation mechanism, acyl-ET2 undergoes a nucleophilic attack from the oxygen atom O_G of GE at the carbon atom C_B of the butyrate group previously inserted at the Ser_{146} side chain. This process takes place with a free energy barrier of 14.0 kcal/mol, associated with transition state $T1_D$. A more sterically crowded gem-diol (I_D) is formed in this process and is endergonic by 4.0 kcal/mol. It is important to note that the nucleophilic attack can also be performed by an adventurous water molecule. Such an event would take the enzyme back to I_A instead of I_D, and it is a known disadvantage of performing esterification reactions in water. Although intermediate I_D is thermodynamically less stable than I_A (with respect to its respective reactants), its collapse occurs with a higher free energy barrier of 8.5 kcal/mol. The higher energy barrier associated with $T2_D$ is due to the presence of the bulky alkyl group, which stabilizes the gem-diol through the electron-donating effect. The collapse of I_D leads to the production of geranyl butyrate and regenerates the free enzyme. The nucleophilic attack step is the rate-limiting step of the deacylation mechanism, which makes the deacylation mechanism the slowest of the two reactions involved in flavor ester production.

In summary, our integrated experimental, statistical, and computational approach evaluated the parameters that most affected the production of geranyl butyrate by ET2 through an esterification reaction. The reaction time was indicated as the most relevant parameter affecting the conversion, followed by the temperature. An increase in the concentration of the acyl acceptor as well as the catalyst load did not enhance the production of the flavor ester significantly. However, at higher levels, an inhibition pattern was observed for these two factors, which negatively affected the conversion. The final experiment performed at the optimum conditions (t = 6 h, T = 50 °C, MR = 1:5, and Cat = 15%) exhibited a conversion of about 93%.

Theoretical studies unveiled the binding modes of each substrate in the active site of ET2. A balance of hydrophobic and hydrophilic forces exerted by resides Ile_{94}, Leu_{154}, and Phe_{265} through weak nonpolar interactions and hydrogen bonding provided by Tyr_{21} are responsible for the stabilization of the enzyme−substrate complex. The nucleophilic attack step of the deacylation reaction was identified as the rate-limiting step of the entire process. That step is associated with a free energy barrier of 14.0 kcal/mol, which is equivalent to a rate constant (k_{cat}) in the order of 10^3 s^{-1}.

Our team is developing a technology to immobilize ET2 for the production of geranyl butyrate as well as other flavor esters, without the use of toxic organic solvents. Preliminary experiments showed an enhancement in the stability of the enzyme and in the reaction rate. This work is now underway and will be reported in due course.

■ ASSOCIATED CONTENT

ⓢ Supporting Information

The Supporting Information is available free of charge at https://pubs.acs.org/doi/10.1021/acsomega.3c08483.

> Chromatogram showing the peak at 220 nm, 1H NMR spectrum of geranyl butyrate, ^{13}C NMR spectrum of geranyl butyrate (highlighting the main peak), comparison of B3LYP and M06-2X DFT functionals, key bond distances in Ångströms for acylation and deacylation reaction mechanisms, and (x, y, z) coordinates of the QM region for each discussed structure in the manuscript (PDF)

■ AUTHOR INFORMATION

Corresponding Author

José Cleiton Sousa dos Santos − *Engineering and Sustainable Development Institute, University of International Integration of Afro-Brazilian Lusophony, Redenção, Ceará 62790-970, Brazil;* ⓘ orcid.org/0000-0002-1511-5180; Phone: +55(85) 9975-23838; Email: jcs@unilab.edu.br

Authors

Francisco Simão Neto − *Department of Chemical Engineering, Federal University of Ceara, Fortaleza, Ceará 60455-760, Brazil*

Paulo Gonçalves de Sousa Junior − *Department of Organic and Inorganic Chemistry, Federal University of Ceara, Fortaleza, Ceará 60440-900, Brazil*

Carlos José Alves da Silva Filho − *Department of Organic and Inorganic Chemistry, Federal University of Ceara, Fortaleza, Ceará 60440-900, Brazil*

Lucas Pinheiro Coutinho − *Department of Analytical Chemistry and Physical Chemistry, Federal University of Ceara, Fortaleza, Ceará 60020-181, Brazil*

Rafael Leandro Fernandes Melo − *Department of Metallurgic Engineering, Federal University of Ceara, Fortaleza, Ceará 60440-554, Brazil*

Javier Rocha-Martin − *Department of Biochemistry and Molecular Biology, Faculty of Biological Sciences, Complutense University of Madrid, Madrid 28040, Spain*

Maria Alexsandra de Sousa Rios − *Department of Mechanical Engineering, Federal University of Ceara, Fortaleza, Ceará 60455-760, Brazil;* ⓘ orcid.org/0000-0002-3145-0456

Ada Amélia Sanders Lopes − *Engineering and Sustainable Development Institute, University of International Integration of Afro-Brazilian Lusophony, Redenção, Ceará 62790-970, Brazil*

Norberto de K. V. Monteiro − *Department of Analytical Chemistry and Physical Chemistry, Federal University of Ceara, Fortaleza, Ceará 60020-181, Brazil;* ⓘ orcid.org/0000-0002-5847-5733

Marcos Carlos de Mattos − *Department of Analytical Chemistry and Physical Chemistry, Federal University of Ceara, Fortaleza, Ceará 60020-181, Brazil;* ⓘ orcid.org/0000-0003-4291-5199

Leonardo Farias Serafim − *Department of Chemistry, Georgia State University, Atlanta, Georgia 30302, United States*

Complete contact information is available at:

https://pubs.acs.org/10.1021/acsomega.3c08483

Notes
The authors declare no competing financial interest.

■ ACKNOWLEDGMENTS

■ REFERENCES

(1) Ferreira, V.; Ortín, N.; Escudero, A.; López, R.; Cacho, J. Chemical Characterization of the Aroma of Grenache Rosé Wines: Aroma Extract Dilution Analysis, Quantitative Determination, and Sensory Reconstitution Studies. *J. Agric. Food Chem.* **2002**, *50* (14), 4048−4054.

(2) Ferreira, V.; López, R.; Cacho, J. F. Quantitative Determination of the Odorants of Young Red Wines from Different Grape Varieties. *J. Sci. Food Agric.* **2000**, *80* (11), 1659−1667.

(3) Verstrepen, K. J.; Derdelinckx, G.; Dufour, J.-P.; Winderickx, J.; Thevelein, J. M.; Pretorius, I. S.; Delvaux, F. R. Flavor-Active Esters: Adding Fruitiness to Beer. *J. Biosci. Bioeng.* **2003**, *96* (2), 110−118.

(4) Koeduka, T.; Fridman, E.; Gang, D. R.; Vassão, D. G.; Jackson, B. L.; Kish, C. M.; Orlova, I.; Spassova, S. M.; Lewis, N. G.; Noel, J. P.; Baiga, T. J.; Dudareva, N.; Pichersky, E. Eugenol and Isoeugenol, Characteristic Aromatic Constituents of Spices, Are Biosynthesized via Reduction of a Coniferyl Alcohol Ester. *Proc. Natl. Acad. Sci. U.S.A.* **2006**, *103* (26), 10128−10133.

(5) SÁ, A. G. A.; Meneses, A. C. D.; Araújo, P. H. H. D.; Oliveira, D. D. A Review on Enzymatic Synthesis of Aromatic Esters Used as Flavor Ingredients for Food, Cosmetics and Pharmaceuticals Industries. *Trends Food Sci. Technol.* **2017**, *69*, 95−105.

(6) Wang, L.; Chen, G.; Tang, J.; Ming, M.; Jia, C.; Feng, B. Continuous Biosynthesis of Geranyl Butyrate in a Circulating Fluidized Bed Reactor. *Food Biosci.* **2019**, *27*, 60−65.

(7) Liu, Y.; WeiZhuo, X.; Wei, X. A Review on Lipase-Catalyzed Synthesis of Geranyl Esters as Flavor Additives for Food, Pharmaceutical and Cosmetic Applications. *Food Chem. Adv.* **2022**, *1*, 100052.

(8) Yushkova, E. D.; Nazarova, E. A.; Matyuhina, A. V.; Noskova, A. O.; Shavronskaya, D. O.; Vinogradov, V. V.; Skvortsova, N. N.; Krivoshapkina, E. F. Application of Immobilized Enzymes in Food Industry. *J. Agric. Food Chem.* **2019**, *67* (42), 11553−11567.

(9) Switzar, L.; Giera, M.; Niessen, W. M. A. Protein Digestion: An Overview of the Available Techniques and Recent Developments. *J. Prot. Res.* **2013**, *12* (3), 1067−1077.

(10) Hasan, F.; Shah, A. A.; Hameed, A. Industrial Applications of Microbial Lipases. *Enzyme Microb. Technol.* **2006**, *39* (2), 235−251.

(11) Kapoor, M.; Gupta, M. N. Lipase Promiscuity and Its Biochemical Applications. *Proc. Biochem.* **2012**, *47* (4), 555−569.

(12) Lan, D.; Zhao, G.; Holzmann, N.; Yuan, S.; Wang, J.; Wang, Y. Structure-Guided Rational Design of a Mono- and Diacylglycerol Lipase from *Aspergillus oryzae*: A Single Residue Mutant Increases the Hydrolysis Ability. *J. Agric. Food Chem.* **2021**, *69* (18), 5344−5352.

(13) Khan, F. I.; Lan, D.; Durrani, R.; Huan, W.; Zhao, Z.; Wang, Y. The Lid Domain in Lipases: Structural and Functional Determinant of Enzymatic Properties. *Front. Bioeng. Biotechnol.* **2017**, *5*, 16.

(14) Polgár, L. Catalytic Mechanisms of Serine and Threonine Peptidases. *Handbook of Proteolytic Enzymes*; Elsevier, 2013; pp 2524−2534.

(15) Chang, M. Y.; Chan, E.-S.; Song, C. P. Biodiesel production catalysed by low-cost liquid enzyme Eversa® Transform 2.0: Effect of free fatty acid content on lipase methanol tolerance and kinetic model. *Fuel* **2021**, *283*, 119266.

(16) Monteiro, R. R. C.; Arana-Peña, S.; da Rocha, T. N.; Miranda, L. P.; Berenguer-Murcia, Á.; Tardioli, P. W.; dos Santos, J. C. S.; Fernandez-Lafuente, R. Liquid Lipase Preparations Designed for Industrial Production of Biodiesel. Is It Really an Optimal Solution. *Renew. Energy* **2021**, *164*, 1566−1587.

(17) de Sousa Junior, P. G.; do Nascimento Camara, A. G.; Oliveira, A. R. T.; de Castro Lima, G.; Lima, G. V.; Coutinho, L. P.; Nunes Holanda Alexandre, J. Y.; Serafim, L. F.; de Mattos, M. C.; de Kássio Monteiro, N. V.; Sousa dos Santos, J. C. Optimization and Theoretical Analysis of Lipase-Catalyzed Enzymatic Esterification of Glycerol for Efficient Glycerides Synthesis. *J. Biochem. Eng.* **2023**, *198*, 109033.

(18) Cavalcante, F. T. T.; da Fonseca, A. M.; Holanda Alexandre, J. Y. N.; dos Santos, J. C. S. A stepwise docking and molecular dynamics approach for enzymatic biolubricant production using Lipase Eversa Transform as a biocatalyst. *Ind. Crops Prod.* **2022**, *187*, 115450.

(19) Alexandre, J. Y. N. H.; Cavalcante, F. T. T.; Freitas, L. M.; Castro, A. P.; Borges, P. T.; de Sousa Junior, P. G.; Filho, M. N. R.; Lopes, A. A. S.; da Fonseca, A. M.; Lomonaco, D.; de Sousa Rios, M. A.; Sousa dos Santos, J. C. A Theoretical and Experimental Study for Enzymatic Biodiesel Production from Babassu Oil (*Orbignya Sp.*) Using Eversa Lipase. *Catalysts* **2022**, *12* (11), 1322.

(20) Brandão Júnior, J.; Andrade do Nascimento, J. G.; França Silva, M. P.; Lima Brandão, E. d. A.; de Castro Bizerra, V.; dos Santos, K. M.; Serpa, J. d. F.; Santos, J. C. S. D.; da Fonseca, A. M.; Vasconcelos de Oliveira, D. L.; Souza, M. C. M. de. Performance of Eversa Transform 2.0 Lipase in Ester Production Using Babassu Oil (*Orbignya Sp.*) and Tucuman Oil (*Astrocaryum vulgar*): A Comparative Study between Liquid and Immobilized Forms in Fe3O4 Nanoparticles. *Catalysts* **2023**, *13* (3), 571.

(21) Taguchi, G. Quality Engineering (Taguchi Methods) for the Development of Electronic Circuit Technology. *IEEE Trans. Reliab.* **1995**, *44* (2), 225−229.

(22) Yu, Y.; Xu, S.; He, R.; Liang, G. Application of Molecular Simulation Methods in Food Science: Status and Prospects. *J. Agric. Food Chem.* **2023**, *71* (6), 2684−2703.

(23) Serafim, L. F.; Jayasinghe-Arachchige, V. M.; Wang, L.; Rathee, P.; Yang, J.; Moorkkannur N, S.; Prabhakar, R. Distinct Chemical Factors in Hydrolytic Reactions Catalyzed by Metalloenzymes and Metal Complexes. *Chem. Commun.* **2023**, *59* (58), 8911−8928.

(24) van der Kamp, M. W.; Mulholland, A. J. Combined Quantum Mechanics/Molecular Mechanics (QM/MM) Methods in Computational Enzymology. *Biochemistry* **2013**, *52* (16), 2708−2728.

(25) Brzozowski, A. M.; Savage, H.; Verma, C. S.; Turkenburg, J. P.; Lawson, D. M.; Svendsen, A.; Patkar, S. Structural Origins of the Interfacial Activation in *Thermomyces (Humicola) Lanuginosa* Lipase. *Biochemistry* **2000**, *39* (49), 15071−15082.

(26) *Gaussian*, 16 Rev. C.01; Wallingford, CT, 2016.

(27) Salomon-Ferrer, R.; Case, D. A.; Walker, R. C. An Overview of the Amber Biomolecular Simulation Package. *Wiley Interdiscip. Rev.: Comput. Mol. Sci.* **2013**, *3* (2), 198−210.

(28) Eberhardt, J.; Santos-Martins, D.; Tillack, A. F.; Forli, S. AutoDock Vina 1.2.0: New Docking Methods, Expanded Force Field, and Python Bindings. *J. Chem. Inf. Model.* **2021**, *61* (8), 3891−3898.

(29) Abraham, M. J.; Murtola, T.; Schulz, R.; Páll, S.; Smith, J. C.; Hess, B.; Lindahl, E. GROMACS: High Performance Molecular Simulations through Multi-Level Parallelism from Laptops to Supercomputers. *SoftwareX* **2015**, *1−2*, 19−25.

(30) Pronk, S.; Páll, S.; Schulz, R.; Larsson, P.; Bjelkmar, P.; Apostolov, R.; Shirts, M. R.; Smith, J. C.; Kasson, P. M.; van der Spoel, D.; Hess, B.; Lindahl, E. GROMACS 4.5: A High-Throughput and Highly Parallel Open Source Molecular Simulation Toolkit. *Bioinformatics* **2013**, *29* (7), 845−854.

(31) Mark, P.; Nilsson, L. Structure and Dynamics of the TIP3P, SPC, and SPC/E Water Models at 298 K. *J. Phys. Chem. A* **2001**, *105* (43), 9954−9960.

(32) Badgujar, K. C.; Pai, P. A.; Bhanage, B. M. Enhanced Biocatalytic Activity of Immobilized *Pseudomonas cepacia* Lipase under Sonicated Condition. *Bioprocess Biosyst. Eng.* **2016**, *39* (2), 211−221.

(33) Badgujar, K. C.; Bhanage, B. M. Enhanced Biocatalytic Activity of Lipase Immobilized on Biodegradable Copolymer of Chitosan and Polyvinyl Alcohol Support for Synthesis of Propionate Ester: Kinetic Approach. *Ind. Eng. Chem. Res.* **2014**, *53* (49), 18806−18815.

(34) Kuo, C.-H.; Chen, G.-J.; Chen, C.-I.; Liu, Y.-C.; Shieh, C.-J. Kinetics and Optimization of Lipase-Catalyzed Synthesis of Rose Fragrance 2-Phenylethyl Acetate through Transesterification. *Proc. Biochem.* **2014**, *49* (3), 437−444.

(35) Geng, B.; Wang, M.; Qi, W.; Su, R.; He, Z. Cinnamyl Acetate Synthesis by Lipase-Catalyzed Transesterification in a Solvent-Free System. *Biotechnol. Appl. Biochem.* **2012**, *59* (4), 270−275.